Light Transition Metal Monatomic Chains

C. Ataca,[1] S. Cahangirov,[2] E. Durgun,[1,2] Y.-R. Jang,[1,3] and S. Ciraci[1,2,*]

[1]*Department of Physics, Bilkent University, Ankara, 06800, Turkey*
[2]*UNAM-Material Science and Nanotechnology Institute, Bilkent University, Ankara 06800, Turkey*
[3]*Department of Physics, University of Incheon, Incheon 402-749, Korea*

(Dated: February 2, 2008)

In this paper we investigated structural, electronic and magnetic properties of *3d* (light) transition metal (TM) atomic chains using first-principles pseudopotential plane wave calculations. Periodic linear, dimerized linear and planar zigzag chain structures and their short segments consisting of finite number of atoms have been considered. Like Cu, the periodic, linear chains of Mn, Co and Ni correspond to a local shallow minimum. However, for most of the infinite periodic chains, neither linear nor dimerized linear structures are favored; to lower their energy the chains undergo a structural transformation to form planar zigzag and dimerized zigzag geometry. Dimerization in both infinite and finite chains are much stronger than the usual Peierls distortion and appear to depend on the number of *3d*-electrons. As a result of dimerization, a significant energy lowering occurs which, in turn, influences the stability and physical properties. Metallic linear chain of Vanadium becomes half-metallic upon dimerization. Infinite linear chain of Scandium also becomes half-metallic upon transformation to zigzag structure. An interplay between the magnetic ground state and atomic as well as electronic structure of the chain has been revealed. The end effects influence the geometry, energetics and magnetic ground state of the finite chains. Structure optimization performed using noncollinear approximation indicates significant differences from the collinear approximation. Variation of the cohesive energy of infinite and finite-size chains with respect to the number of *3d*-electrons are found to mimic the bulk behavior pointed out by Friedel. The spin-orbit coupling of finite chains are found to be negligibly small.

PACS numbers: 73.63.Nm, 75.50.Xx, 75.75.+a

I. INTRODUCTION

Fabrication of nanoscale structures, such as quantum dots, nanowires, atomic chains and functionalized molecules have made a great impact in various fields of science and technology.[1,2,3,4] Size and dimensionality have been shown to strongly affect the physical and chemical properties of matter.[5] Electrons in lower dimensionality undergo a quantization which is different from that in the bulk materials.[6,7,8] In nanoscale size, the quantum effects, in particular the discrete nature of electronic energies with significant level spacing are pronounced.

Suspended monoatomic chains being an ultimate one-dimensional (1D) nanowire have been produced and their fundemental properties both theoretically and experimentally investigated.[9,10,11,12,13,14,15,16,17,18,19] Ballistic electron transport[6] with quantized conductance at room temperature has been observed in metallic nanowires.[9,15] Moreover, magnetic and transport properties become strongly dependent on the details of atomic configuration. Depending on the type and position of a foreign atom or molecule that is adsorbed to a nansostructure, dramatic changes can occur in the physical properties.[3] Some experimental studies, however, aimed at producing atomic chains on a substrate.[20] Here the substrate-chain interaction can enter as a new degrees of freedom to influence the physical properties.

Unlike the metal and semiconductor chains, not many theoretical studies are performed on transition metal[21,22,23,24] (TM) monatomic chains. TM monatomic chains have the ability to magnetize much more than the bulk.[25] Large exchange interactions of TM atoms in the bulk are overcame by the large electron kinetic energies, which result in a nonmagnetic ground state with large bandwidth. On the other hand, geometries which are nonmagnetic in bulk may have magnetic ground states in monatomic chains.[25] In addition, it is predicted that the quantum confinement of electrons in metallic chains should result in a magnetic ground state and also a super paramagnetic state for some of the TM chains[26] at finite temperatures. The central issue here is the stability of the chain and the interplay between 1D geometry and magnetic ground state.[21,24]

From the technological point of view, TM monatomic chains are important in spin dependent electronics, namely spintronics.[27] While most of the conventional electronics is based on the transport of information through charges, future generation spintronic devices will take the advantage of the electron spin to double the capacity of electronics. It has been revealed that TM atomic chains either suspended or adsorbed on a 1D substrate, such as carbon nanotubes or Si nanowires can exhibit high spin-polarity or half-metallic behavior relevant the for spin-valve effect.[3] Recently, first-principles pseudopotential calculations have predicted that the finite size segments of linear carbon chains capped by specific *3d*-TM atoms display an interesting even-odd disparity depending on the number of carbon atoms. For example, CoC_nCo linear chain has an antiferromagnetic ground state for even n, but the ground state changes to ferromagnetic for odd n. Even more interesting is the fer-

romagnetic excited state of an antiferromagnetic ground state can operate as a spin-valve when CoC_nCo chain is connected to metallic electrodes from both ends.[28]

As the chain length decreases, finite-size effects dominate the magnetic and electronic properties.[21,29] When compared with the infinite case, these are less stable to thermal fluctuations.[30] Additional effects on the behavior of nanoparticle are their intrinsic properties and the interaction between them.[29,30,31,32] Effects of noncollinear magnetism have to be taken into account as well.[33,34,35] The end atoms also exhibit different behavior with respect to the atoms close to the middle of the structure.[36]

In this paper, we consider infinite, periodic chains of *3d*-TM atoms having linear and planar zigzag structures and their short segments consisting of finite number of atoms. For the sake of comparison, Cu and Zn chains also included in our study. All the chain structures discussed in this paper do not correspond to a global minimum, but may belong to a local minimum. The infinite and periodic geometry is of academic interest and can also be representative for very long monatomic chains. The main interest is, however, the short segments comprising finite number of TM atoms. We examined the variation of energy as a function of the lattice constant in different magnetic states, and determined the stable infinite and also finite-size chain structures. We investigated the electronic and magnetic properties of these structures. Present study revealed a number of properties of fundamental and technological interest: The linear geometry of the infinite, periodic chain is not stable for most of the *3d*-TM atoms. Even in the linear geometry, atoms are dimerized to lower the energy of the chain. We found that infinite linear Vanadium chains are metallic, but become half-metallic upon dimerization. The planar zigzag chains are more energetic and correspond to a local minimum. For specific TM chains, the energy can further be lowered through dimer formation within planar zigzag geometry. Dramatic changes in electronic properties occur as a result of dimerization. Magnetic properties of short monatomic chains have been investigated using both collinear and noncollinear approximation, which are resulted in different net magnetic moment for specific chains. Spin-orbit coupling which are calculated for different direction of applied magnetic field have been found to be negligibly small.

II. METHODOLOGY

We have performed first-principles plane wave calculations[37,38] within Density-Functional Theory (DFT)[39] using ultra-soft pseudopotentials.[40] We also used PAW[41] potentials for noncollinear and noncollinear spin-orbit calculations of finite chains. The exchange-correlation potential has been approximated by generalized gradient approximation (GGA).[42] For partial occupancies, we have used the Methfessel-Paxton smearing method.[43] The width of smearing for infinite structures has been chosen as 0.1 eV for geometry relaxations and as 0.01 eV for accurate energy band and density of state (DOS) calculations. As for finite structures, the width of smearing is taken as 0.01 eV. We treated the chain structures by supercell geometry (with lattice parameters a_{sc}, b_{sc}, and c_{sc}) using the periodic boundary conditions. A large spacing ($\sim 10\mathring{A}$) between adjacent chains has been assured to prevent interactions between them. In single cell calculations of infinite systems, c_{sc} has been taken to be equal to the lattice constant of the chain. The number of plane waves used in expanding Bloch functions and **k**-points used in sampling the Brillouin zone (BZ) have been determined by a series of convergence tests. Accordingly, in the self-consistent potential and total energy calculations the BZ has been sampled by (1x1x41) mesh points in **k**-space within Monkhorst-Pack scheme.[44] A plane-wave basis set with kinetic energy cutoff $\hbar^2|\mathbf{k}+\mathbf{G}|^2/2m = 350\ eV$ has been used. In calculations involving PAW potentials, kinetic energy cutoff is taken as 400 eV. All atomic positions and lattice constants (c_{sc}) have been optimized by using the conjugate gradient method where total energy and atomic forces are minimized. The convergence is achieved when the difference of the total energies of last two consecutive steps is less than 10^{-5} eV and the maximum force allowed on each atom is 0.05 eV/$\mathring{A}$. As for finite structures, supercell has been constructed in order to assure $\sim 10\mathring{A}$ distance between the atoms of adjacent finite chain in all directions and BZ is sampled only at the Γ-point. The other parameters of the calculations are kept the same. The total energy of optimized structure (E_T) relative to free atom energies is negative, if they are in a binding state. As a rule, the structure becomes more energetic (or stable) as its total energy is lowered. Figure 1 describes various chain structures of TM atoms treated in this study. These are infinite periodic chains and segments of a small number of atoms forming a string or a planar zigzag geometry. The stability of structure-optimized finite chains are further tested by displacing atoms from their equilibrium positions in the plane and subsequently reoptimizing the structure. Finite-size clusters of TM atoms are kept beyond the scope of this paper.

III. INFINITE AND PERIODIC CHAIN STRUCTURES

In Fig. 2, we present the energy versus lattice constant of various infinite and periodic chain structures (described in Fig. 1) in different magnetic states. In calculating the ferromagnetic (FM) state, the structure is optimized each time using a spin-polarized GGA calculations starting with a different preset magnetic moment in agreement with Hund's rule. The relaxed magnetic moment yielding to the lowest total energy has been taken

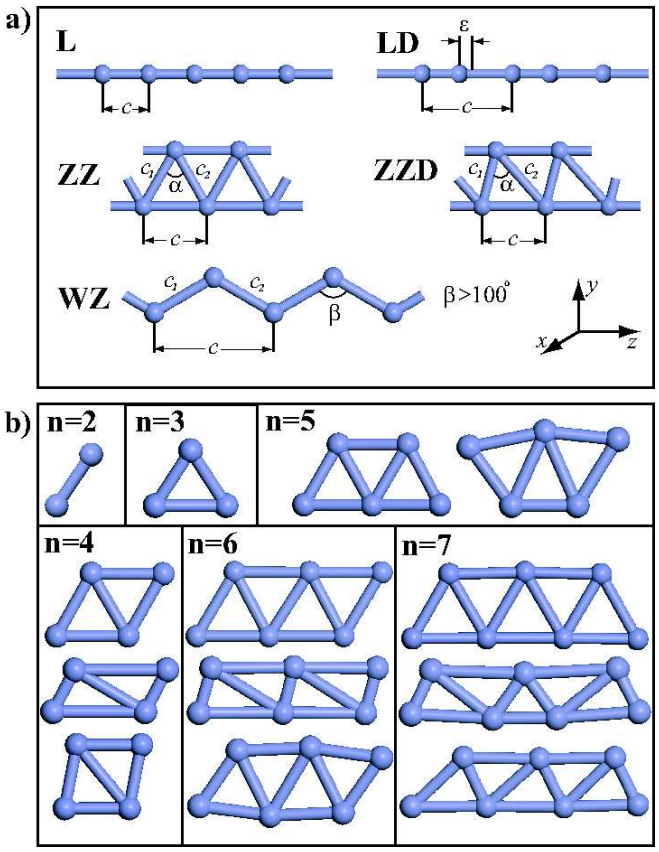

FIG. 1: (Color online) Various structures of *3d*-TM atomic chains. (a) Infinite and periodic structures; L: The infinite linear monatomic chain of TM atom with lattice constant, c. LD: The dimerized linear monatomic chain with two TM atoms in the cell. ϵ is the displacement of the second atom from the middle of the unit cell. ZZ: The planar zigzag monatomic chain with lattice parameter c and unit cell having two TM atoms. $c_1 \sim c_2$ and $59^0 < \alpha < 62^0$. ZZD: The dimerized zigzag structure $c_1 \neq c_2$. WZ: The wide angle zigzag structure $c_1 \sim c_2$, but $\alpha > 100^0$. (b) Various chain structures of small segments consisting of finite number (n) of TM atoms, denoted by $(TM)_n$.

as the FM state of the chain. For the antiferromagnetic (AFM) state, we assigned different initial spins of opposite directions to adjacent atoms and relaxed the structure. We performed spin-unpolarized GGA calculations for the nonmagnetic (NM) state. The energy per unit cell relative to the constituent free atoms is calculated from the expression, $E = [NE_a - E_T]$, in terms of the total energy per unit cell of the given chain structure for a given magnetic state (E_T) and the ground state energy of the free constituent TM atom, E_a. N is the number of TM atom in the unit cell, that is N=1 for L, but N=2 for LD, ZZ, and ZZD structures. The minimum of E is the binding energy. By convention $E_b < 0$ corresponds to a binding structure, but not necessary to a stable structure. The cohesive energy per atom is $E_c = -E_b/N$. Light transition metal atoms can have different structural and magnetic states depending on the number of their *3d* electrons. For example, Sc having a single *3d* electron, has a shallow minimum corresponding to a dimerized linear chain structure in the FM state. If the L structure is dimerized to make a LD structure, the energy of the chain is slightly lowered. Other linear structures, such as linear NM, and AFM have higher energy. More stable structure ZZ is, however, in the FM state. The situation is rather different for Cr, Fe, and Mn. For example, Cr have LD and more energetic ZZD structures in the AFM state. It should be noted that in the dimerized linear chain structure of Cr the displacement of the second atom from the middle of the unit cell, ϵ, is rather large. Apparently, the dimerization is stronger than the usual Peierls distortion. As a result, the nearest neighbor distance, $(c - \epsilon)$, is much smaller than the second nearest neighbor distance, $(c + \epsilon)$. This situation poses the question whether the interaction between the adjacent dimers are strong enough to maintain the coherence of the chain structure. We address this question by comparing the energies of individual dimers with the chain structure. The formation of the LD structure is energetically more favorable with respect to individual dimer by 0.54 eV per atom. Furthermore, the charge density contour plots presented in Fig. 3 indicate a significant bonding between adjacent dimers. Nevertheless, the LD structure has to transform to more energetic ZZD structure. The zigzag structures in the AFM, FM and NM states have minima at higher binding energies and hence are unstable. The linear and LD Fe chains have a local minimum in FM state. More stable ZZ and ZZD structures in FM state have almost identical minima in lower binding energy. The most stable chain structure of Mn among ones described in Fig. 2 is ZZ in FM state. It is also saliency to note that both Fe and Mn chains in NM state undergo a structural transformation from ZZ to WZ structure. It is noted from Fig. 2 that the structure of *3d*-TM atomic chains are strongly dependent on their magnetic state. Optimized structural parameters, cohesive energy, magnetic state and net magnetic moment of infinite linear and zigzag structures are presented in Table I and Table II, respectively.

In Fig. 4 and Fig. 5 we compare the nearest neighbor distance and the average cohesive energy of the linear and zigzag chain structures with those of the bulk metals and plot their variations with respect to their number of *3d* electrons of the TM atom. The nearest neighbor distance in the linear and zigzag structures are smaller than that of the corresponding bulk structure, but display the similar trend. Namely, it is large for Sc having a single *3d* electron and decreases as the number of *3d* electrons, *i.e.* N_d, increases to four. Mn is an exception, since the bulk and the chain structure show opposite behavior. While the nearest neighbor distance of bulk Mn is a minimum, it attains a maximum value in the chain structure. Owing to their smaller coordination number,

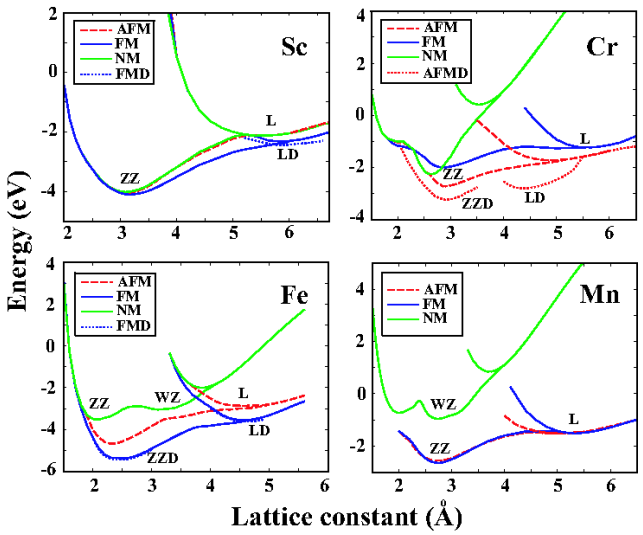

FIG. 2: (Color online) The energy versus lattice constant, c, of various chain structures in different magnetic states. FM: ferromagnetic; AFM: antiferromagnetic; NM: nonmagnetic; FMD: ferromagnetic state in the linear or zigzag dimerized structure; AFMD: antiferromagnetic state in the dimerized linear or zigzag structure. The energy is taken as the energy per unit cell relative to the constituent free atom energies in their ground state (See text for definition). In order to compare the energy of the L structure with that of the LD, the unit cell (and also lattice constant) of the former is doubled in the plot. Types of structures identified as L, LD, ZZ, ZZD, WZ are describes in Fig. 1.

	Sc	Ti	V	Cr	Mn	Fe	Co	Ni	Cu	Zn
c	6.0	4.9	4.5	4.4	2.6	4.6	2.1	2.2	2.3	2.6
ε	0.38	0.52	0.51	0.66	0.0	0.21	0.0	0.0	0.0	0.0
E_c	1.20	1.83	1.86	1.40	0.76	1.81	2.10	1.99	1.54	0.15
MGS	FM	FM	FM	AFM	AFM	FM	FM	FM	NM	NM
μ	1.74	0.45	1.00	±1.95	±4.40	3.32	2.18	1.14	0.0	0.0

TABLE I: The calculated values for linear structures (L and LD). The lattice constant, c (in Å); the displacement of the second atom in the unit cell of dimerized linear structure, ϵ (in Å); cohesive energy, E_c (in eV/atom); the magnetic ground state, MGS; and the total magnetic moment, μ per unit cell (in Bohr magnetons, μ_B) obtained within collinear approximation.

chain structures have smaller cohesive energy as compared to the bulk crystals as shown in Fig. 5. However, both L (or LD if it has a lower energy) and ZZ (or ZZD if it has a lower energy) also show the well-known double hump behavior which is characteristics of the bulk TM crystals. Earlier, this behavior was explained for the bulk TM crystals.[4,45,46] The cohesive energy of zigzag structures are generally ~ 0.7 eV larger than that of the linear structures. However, they are 1-2 eV smaller than that of the bulk crystal. This implies that stable chain structures treated in this study correspond only to local

	Sc	Ti	V	Cr	Mn	Fe	Co	Ni	Cu	Zn
c	3.17	2.60	2.60	2.90	2.76	2.40	2.30	2.30	2.40	2.50
c_1	2.94	2.43	1.84	1.57	2.64	2.24	2.23	2.33	2.39	2.67
c_2	2.94	2.45	2.42	2.65	2.64	2.42	2.39	2.33	2.39	2.67
α	65.2	64.5	73.8	82.6	63.0	61.9	59.6	59.1	60.2	55.8
E_c	2.05	2.78	2.64	1.57	1.32	2.69	2.91	2.74	2.16	0.37
MGS	FM	FM	NM	AFM	FM	FM	FM	FM	NM	NM
μ	0.99	0.18	0.0	±1.82	4.36	3.19	2.05	0.92	0.0	0.0

TABLE II: The calculated values for the planar zigzag structures (ZZ and ZZD): The lattice constant, c (in Å); the first nearest neighbor, c_1 (in Å); the second nearest neighbor, c_2 (in Å); angle between them, α (in degrees); the cohesive energy, E_c (in eV/atom); the magnetic ground state, MGS; and the total magnetic moment, μ per unit cell (in Bohr magnetons, μ_B) obtained within collinear approximation.

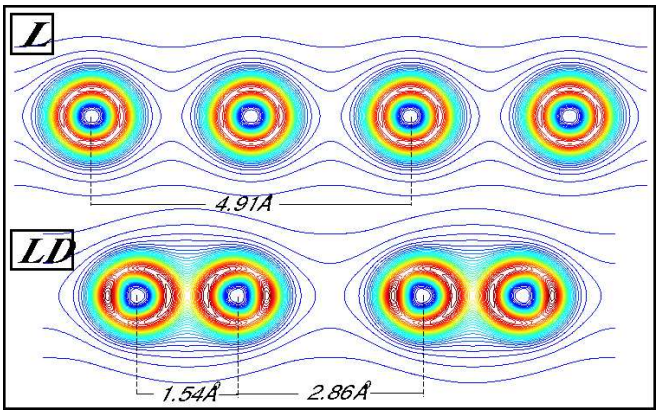

FIG. 3: (Color online) Charge density contour plots for the linear (L) and the dimerized linear structure (LD) of Cr monatomic chains. Interatomic distances are indicated. Contour spacings are equal to $\Delta\rho = 0.0827e/Å^3$. The outermost contour corresponds to $\Delta\rho = 0.0827e/Å^3$.

minima in the Born-Oppenheimer surface.

We note that spin-polarized calculations are carried out under collinear approximation. It is observed that all chain structures presented in Table I and Table II have magnetic state if $N_d < 9$. Only Cr and Mn linear chain structures and Cr zigzag chain structure have an AFM lowest energy state. The binding energy difference between the AFM state and the FM state, $\Delta E = E_b^{AFM} - E_b^{FM}$, is calculated for all light TMs. Variation of ΔE with N_d is plotted in Fig. 6. We see that only Cr ZZ and ZZD chains have an AFM lowest energy state. ΔE of Fe is positive and has the largest value among all *3d*-TM zigzag chains. Note that ΔE increases significantly as a result of dimerization.

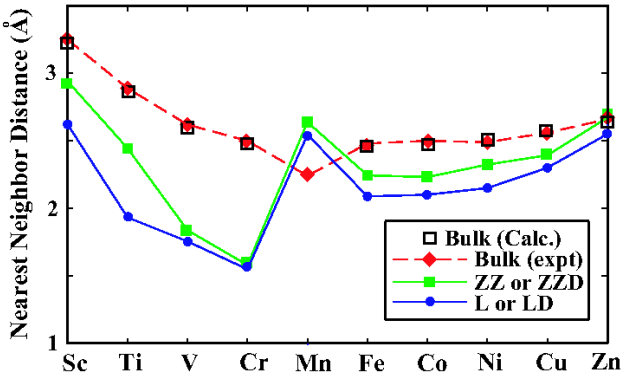

FIG. 4: (Color online) Variation of the nearest neighbor distance of *3d*-TM atomic chains and the bulk structures. For the linear and zigzag structures the lowest energy configuration (i.e. symmetric or dimerized one) has been taken into account. Experimental values of the bulk nearest neighbor distances have been taken from Ref.[47].

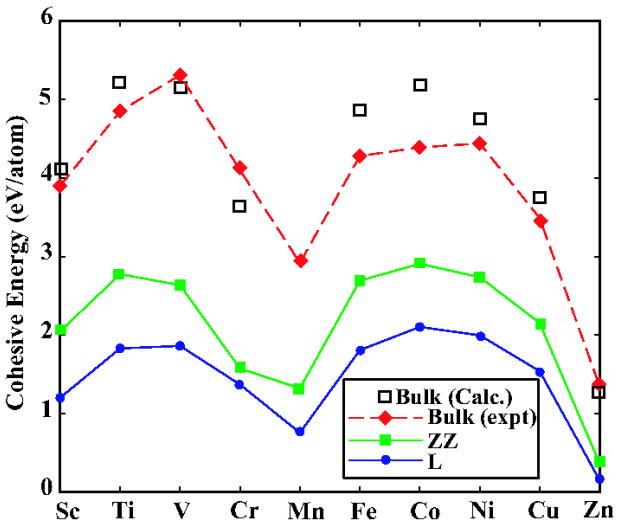

FIG. 5: (Color online) Variation of the cohesive energy, E_c (per atom), of *3d*-TM monatomic chains in their lowest energy linear, zigzag and bulk structures. For the linear and zigzag structures the highest cohesive energy configuration (i.e. symmetric or dimerized one) has been taken into account. Experimental values of the bulk cohesive energies have been taken from Ref.[47]

Having discussed the atomic structure of *3d*-TM chains, we next examine their electronic band structure. In Fig. 7, the chain structures in the first column do not dimerize. The linear chains placed in the third column are dimerized and changed from the L structure in the second column to form the LD structure. Most of the linear structures in Fig. 7 display a FM metallic character with broken spin degeneracy. A few exceptions

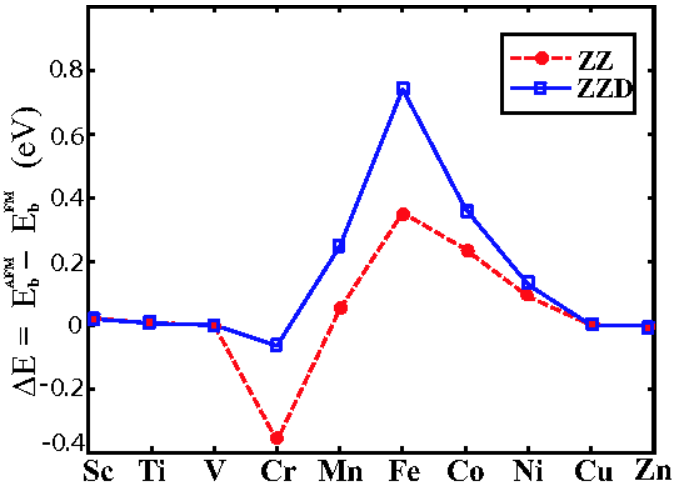

FIG. 6: (Color online) Variation of the binding energy difference, ΔE (per atom) between the lowest antiferromagnetic and ferromagnetic states of *3d*-TM monatomic chains. Open squares and filled circles are for the symmetric zigzag ZZ and dimerized zigzag ZZD chains respectively.

are Mn, Cr, and V chains. The linear Mn chain has an AFM state, where spin-up (majority) and spin-down (minority) bands coincide. Chromium L and LD structures are AFM semiconductors. Vanadium is a ferromagnetic metal for both spins, but becomes half-metallic upon dimerization. In half-metallic state, the chain has integer number of net spin in the unit cell. Accordingly, Vanadium chain in the LD structure is metallic for one spin direction, but semiconducting for the other spin direction. Hence, the spin polarization at the Fermi level, *i.e.* $P = [D_\uparrow(E_F) - D_\downarrow(E_F)]/[D_\uparrow(E_F) + D_\downarrow(E_F)]$ is 100%. Bands of Cu and Zn with filled *3d*-shell in nonmagnetic state are in agreement with previous calculations.[48] In Fig. 8, the chain structures in the first column have only ZZ structure. The zigzag chains in the second column are transformed to a lower energy (*i.e.* more energetic) ZZD structure in the third column. The ZZ chain of Sc is stable in a local minimum and displays a half-metallic character with 100% spin-polarization at the Fermi level. Accordingly, a long segment of ZZ chain of Sc can be used as a spin-valve. Ti, Mn, and Ni in their stable zigzag structures are FM metals. The stable ZZD structure of Fe and Co chains are also FM metals. The ZZ and relatively lower energy ZZD structure of V chain are nonmagnetic. Both ZZ and ZZD structures of Cr are in the AFM state.

For Co and Fe in the ZZD structure more bands of one type of spin cross the Fermi level as compared to those of the other type of spin resulting in a high spin-polarization at the Fermi level. This situation implies that in the ballistic electron transport, the conductance of electrons with one type of spin is superior to electrons with the opposite type of spin; namely $\sigma_\downarrow \gg \sigma_\uparrow$.

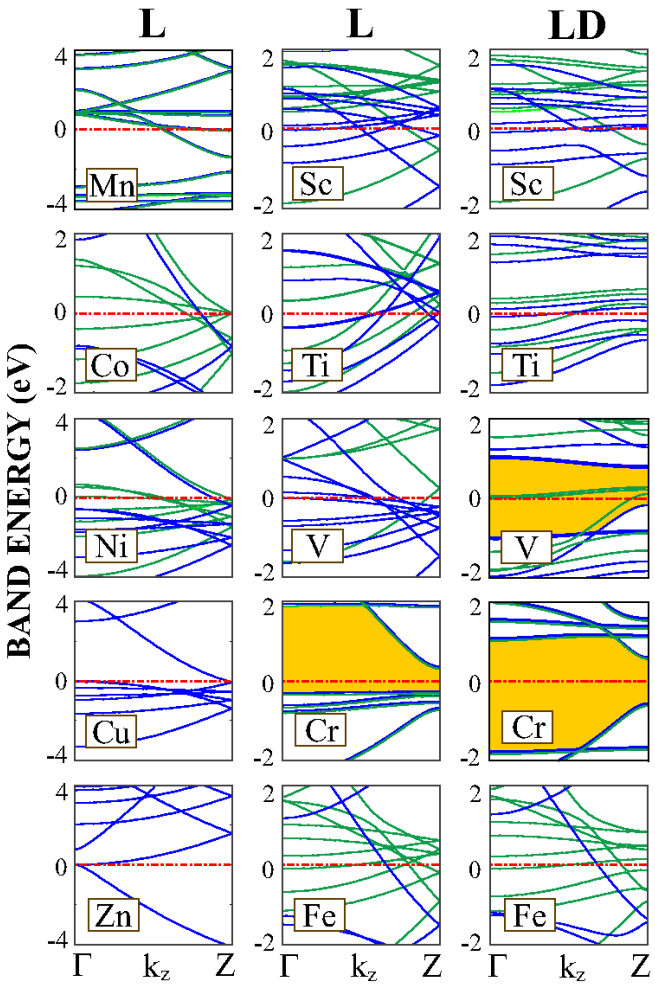

FIG. 7: (Color online) Energy band structures of *3d*-TM atomic chains in their L and LD structures. The zero of energy is set at the Fermi level. Gray and black lines are minority and majority bands, respectively. In the antiferromagnetic state majority and minority bands coincide. Energy gaps between the valence and the conduction bands are shaded.

Accordingly, the conductance of electrons across the Fe and Co chains becomes strongly dependent on their spin-directions. This behavior of the infinite periodic Fe or Co chain is expected to be unaltered to some extend for long, but finite chains and can be utilized as a spin-dependent electronic device. In closing this section, we emphasized that the infinite, periodic chains of *3d*-TM atoms can be in the zigzag structure corresponding to a local minimum. However, most of the zigzag structures are dimerized. Dimerization causes remarkable changes in electronic and magnetic properties.

IV. SHORT CHAIN STRUCTURES

Periodic infinite chains in Section III are only ideal structures; long finite-size segments perhaps can attain

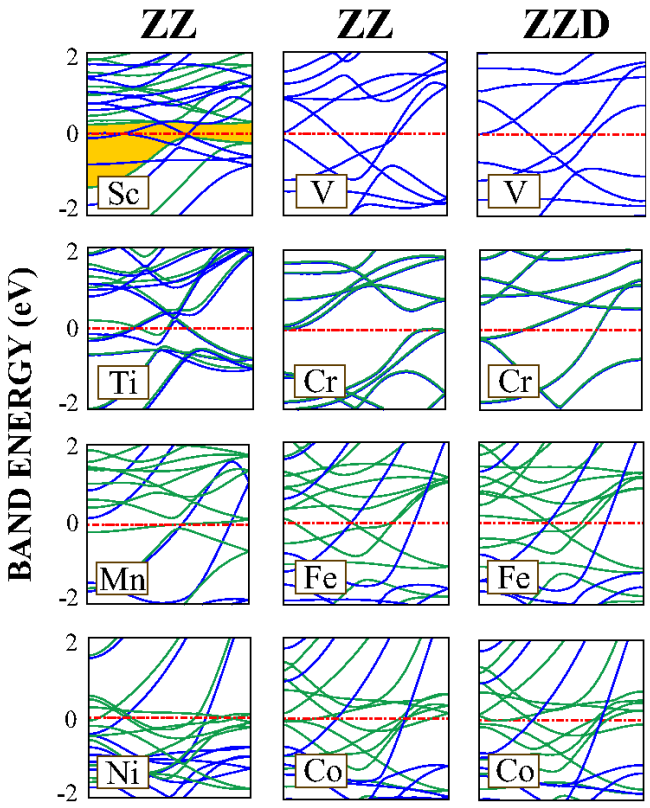

FIG. 8: (Color online) Energy band structures of *3d*-TM atomic chains in their zigzag (ZZ) and dimerized zigzag (ZZD) structures. The zero of energy is set at the Fermi level. Gray and black lines are minority and majority spin bands, respectively. The gray and dark lines coincide in the antiferromagnetic state. Only dark lines describe the bands of nonmagnetic state. The energy gap between the valence and the conduction bands is shaded.

their physical properties revealed above. On the other hand, the end effects can be crucial for short segments consisting of few atoms which may be important for various spintronic applications. In this section, we examine short segments of *3d*-TM chains consisting of n atoms, where n=2-7.

A. Collinear Approximation

We first study the atomic structure and magnetic properties of the finite chains within collinear approximation using ultra-soft pseudopotentials.[40] The linear structure is unstable for the finite size segments. Various planar zigzag structures, which are only a local minima, are described in Fig. 1. We optimized the geometry of these zigzag structures with different initial conditions of magnetic moment on the atoms within collinear approximation. If the final optimized structures for q different initial conditions result in different average cohesive energy (or different total energy), they may actually trapped

in different local minima. Here we considered following different initial conditions: (1) At the beginning, opposite magnetic moments, $\pm\mu_a$, have been assigned to adjacent atoms, and the total magnetic moment, $\mu = \sum \mu_a$, has been forced to vanish at the end of optimization for $n = 2 - 7$. Initial magnetic moment, μ_a, on atoms are determined from the Hund's rule. (2) For $n = 2 - 7$, initial magnetic moment of all atoms have been taken in the same direction, but the final magnetic moment of the structure has been determined after optimization without any constraint. (3) For $n = 2 - 7$, the system is relaxed using spin-unpolarized GGA. (4) For $n = 2 - 7$, initial magnetic moment of chain atoms have been assigned as is done in (1), but $\mu = \sum \mu_a$ is not forced to vanish in the course of relaxation. (5) For $n = 2 - 7$, spin-polarized GGA calculations have been carried out without assigning any initial magnetic moment. (6) We have assigned the magnetic moment $\uparrow\downarrow \quad \downarrow\uparrow$ for $n = 4$, and $\uparrow\downarrow \quad \downarrow \quad \downarrow\uparrow$ for $n = 5$. Here different spacings between two spin-arrows indicate different bond lengths. This way different exchange coupling for different bond lengths and hence dimerization is accounted. (7) The initial magnetic moment on atoms $\uparrow\downarrow \quad \downarrow\uparrow \quad \uparrow\downarrow$ for $n = 6$ and $\uparrow\downarrow\uparrow \quad \uparrow \quad \uparrow\downarrow\uparrow$ for $n = 7$ have been assigned. (8) Similar to (7), initial magnetic moment $\uparrow\downarrow\uparrow \quad \uparrow\downarrow\uparrow$ and $\uparrow\downarrow \quad \downarrow\uparrow\downarrow \quad \downarrow\uparrow$ have been assigned for n=6 and n=7, respectively. Last three initial conditions are taken into consideration due to the fact that different bond lengths of *3d*-TM atoms affect the type of magnetic coupling between consecutive atoms.[24] The initial atomic structures have been optimized for these initial conditions except Cu and Zn. Only first three conditions are consistent with Cu and Zn. As the initial geometry, a segment of n atoms has been extracted from the optimized infinite zigzag chain and placed in a supercell, where the interatomic distance between adjacent chains was greater than 10 Å for all atoms. Our results are summarized in Table III, where the magnetic orders having the same lowest total energy occurred p times from q different initial conditions, are presented. In this respect the magnetic ordering in Table III may be a potential candidate for the magnetic ground state.

The average cohesive energy of finite-size chains increase with increasing n. In Fig. 9, we plot the average cohesive energy of these small segments consisting of n atoms. For the sake of comparison, we presented the plots for the linear and zigzag structures. The average values of cohesive energy in Fig. 9(b) are taken from Table III. We note three important conclusions drawn from these plots. (i) The cohesive energies of the zigzag structures are consistently larger than those of the linear structures, and the cohesive energies also increase with increasing n. (ii) For each types of structures, as well as for each n, the variation of E_c with respect to the number of *3d* electrons in the outer shell, N_d, exhibits a double hump shape, which is typical of the bulk and the infinite chain structures as presented in Fig. 5. (iii) For specific cases $E_c(n_2) < E_c(n_1)$, even if $n_2 > n_1$ (V and Cr). This situation occurs because energy cannot be lowered in the absence of dimerization.

Most of the finite zigzag chain structure of *3d*-TM atoms have a FM lowest energy state. The magnetic ordering specified by AFM* for specific chains indicates that the magnetic moment on individual atoms, μ_a, may be in opposite directions or may have unequal magnitudes, but the total magnetic moment, $\mu = \sum \mu_a$, adds up to zero. The finite chains of Zn atom are always nonmagnetic for all n. Finite zigzag chains of Cu are nonmagnetic for even n, except $n = 6$. Interestingly, the dimerized linear chain of Cr ($n = 5$) with a FM lowest energy state is more energetic than that of the zigzag chain given in Table III. The geometry of this structure is such that two dimers consisting of two atoms are formed at both ends of the linear structure and a single atom at the middle is located equidistant from both dimers. The distance from the middle atom to any of the dimers is approximately twice of the distance between the atoms in the dimer. Even though the nearest neighbor distance of the middle atom to dimers is long, there is a bonding between them. The cohesive energy is ~ 0.2 eV higher than that of the zigzag case, and the total magnetic moment of the structure (6 μ_B) is provided by the atom at the middle. This is due to the fact that two dimers at both ends are coupled in the AFM order. This is an expected result because the cohesive energy (per atom) of Cr_2 is higher than that of Cr_5 in the zigzag structure. The LUMO/HOMO gap for majority and minority spin states usually decrease with increasing n. However, depending of the type of TM atom, the maximum value of the gap occurs for different number of atoms n. The zigzag chain of Zn atoms usually have the largest gap for a given n.

Even though the total magnetic moment, $\mu = \sum \mu_a$, of the AFM* state vanishes for the finite molecule, LUMO-HOMO gaps for majority and minority states are not generally the same as in the AFM state. This can be explained by examining the magnetic moment on every individual atom and the geometry of the molecule. For Cr_4, the magnetic moment on each atom are lined up as described in the sixth initial condition. In this ordering, two dimers each consisting of two atoms are in the AFM ordering within themselves, but in the FM ordering with each other. The distribution of final magnetic moment on atoms for Mn_6 also obey one of the initial conditions (case 7). Three dimers each consisting of two atoms coupled in the AFM order within themselves, but in the FM order

TABLE III: The average cohesive energy E_c (in eV/atom); the net magnetic moment μ, (in Bohr magneton μ_B); magnetic ordering (MO); LUMO-HOMO gap of majority/minority states, $E_G^{\uparrow}$ and $E_G^{\downarrow}$, respectively (in eV) for lowest energy zigzag structures. p/q indicates that the same optimized structure occurred p times starting from q different initial conditions.(See text) Results have been obtained by carrying out structure optimization within collinear approximation using the ultra-soft pseudopotentials.

ZZ		Sc	Ti	V	Cr	Mn	Fe	Co	Ni	Cu	Zn
$n=2$	E_c	0.83	1.38	1.29	0.93	0.32	1.29	1.49	1.38	1.14	0.02
	μ	4.0	2.0	2.0	0.0	10.0	6.0	4.0	2.0	0.0	0.0
	$E_G^{\uparrow}/E_G^{\downarrow}$	0.59/1.60	0.29/1.01	1.03/1.22	2.17/2.17	2.04/0	1.14/0.59	1.42/0.36	1.48/0.27	1.59/1.59	3.96/3.96
	MO	FM	FM	FM	AFM	FM	FM	FM	FM	NM	NM
	$(p/q=5)$	2	1	2	1	1	2	2	1	3	3
$n=3$	E_c	1.30	1.87	1.61	0.91	0.63	1.72	1.84	1.78	1.24	0.12
	μ	1.0	6.0	3.0	6.0	15.0	10.0	7.0	2.0	1.0	0.0
	$E_G^{\uparrow}/E_G^{\downarrow}$	0.66/0.44	0.45/1.08	0.31/0.78	1.23/2.03	1.66/0.35	0.39/0.58	0.19/0.18	0.87/0.24	0.08/1.55	2.96/2.96
	MO	FM	FM	FM	FM	FM	FM	FM	FM	FM	NM
	$(p/q=5)$	3	1	2	2	1	2	3	3	1	3
$n=4$	E_c	1.54	2.13	2.01	1.16	0.84	2.07	2.31	2.08	1.61	0.13
	μ	4.0	2.0	2.0	0.0	18.0	14.0	10.0	4.0	0.0	0.0
	$E_G^{\uparrow}/E_G^{\downarrow}$	0.37/0.36	0.46/0.50	0.35/0.30	1.16/0.61	1.16/0.50	1.47/0.04	1.98/0.34	1.10/0.25	0.96/0.96	2.35/2.35
	MO	FM	FM	FM	AFM*	FM	FM	FM	FM	NM	NM
	$(p/q=6)$	5	3	4	4	4	2	1	3	3	3
$n=5$	E_c	1.63	2.27	2.08	0.83	0.91	2.25	2.46	2.23	1.74	0.15
	μ	3.0	0.0	0.0	0.0	5.0	16.0	11.0	6.0	1.0	0.0
	$E_G^{\uparrow}/E_G^{\downarrow}$	0.29/0.46	0.43/0.43	0.49/0.40	0.47/0.52	1.12/0.30	1.42/0.56	1.53/0.37	1.47/0.09	1.42/0.90	1.96/1.96
	MO	FM	AFM*	AFM*	AFM*	FM	FM	FM	FM	FM	NM
	$(p/q=6)$	3	4	2	4	4	1	1	3	1	3
$n=6$	E_c	1.69	2.32	2.26	1.29	1.02	2.31	2.50	2.29	1.75	0.17
	μ	8.0	0.0	0.0	0.0	0.0	20.0	14.0	6.0	2.0	0.0
	$E_G^{\uparrow}/E_G^{\downarrow}$	0.22/0.29	0.44/0.44	0.54/0.54	0.53/0.55	0.41/0.38	1.33/0.41	0.30/0.32	0.28/0.10	1.42/0.95	1.88/1.88
	MO	FM	AFM	AFM	AFM*	AFM*	FM	FM	FM	FM	NM
	$(p/q=7)$	3	3	7	4	4	2	4	4	1	3
$n=7$	E_c	1.74	2.38	2.22	1.25	1.06	2.35	2.58	2.36	1.84	0.18
	μ	7.0	6.0	5.0	6.0	5.0	22.0	15.0	8.0	1.0	0.0
	$E_G^{\uparrow}/E_G^{\downarrow}$	0.01/0.33	0.34/0.21	0.32/0.48	0.54/0.68	0.85/0.42	0.95/0.29	0.98/0.17	0.83/0.09	0.79/0.61	1.77/1.77
	MO	FM	FM	FM	FM	FM	FM	FM	FM	FM	NM
	$(p/q=7)$	5	3	6	4	5	1	2	4	1	3

with each other. Similar results are also obtained for other AFM* states.

The zigzag planar structure for $n > 3$ in Table III corresponds to a local minimum. To see whether the planar zigzag structures are stable, or else it transforms to other geometry by itself is a critical issue. To assure that the finite chain structures of $n = 4$ and $n = 7$ in Table III are stable in a local minimum, we first displaced the atoms out of planes, then we optimized the structure. Upon relaxation all displaced atoms returned to their equilibrium position on the plane.

B. Noncollinear approximation and the spin-orbit interaction

In cases where both AFM and FM couplings occur and compete with each other, collinear magnetism fails for modelling the ground state magnetic ordering. A midway between AFM and FM exchange interactions results in allowing the spin quantization axis to vary in every site of the structure. Geometric structure also influences non-

TABLE IV: The average cohesive energy, E_c(in eV/atom); the components (μ_x, μ_y, μ_z) and the magnitude of the net magnetic moment μ (in μ_B); LUMO-HOMO gap E_G (in eV) / energy gap under 1 μ_B applied magnetic field along x-direction(/z-direction) E_G^x/E_G^z; magnetic ordering MO; Spin-orbit coupling energy $\triangle E_{so}^x(/\triangle E_{so}^z)$ (in meV) under applied magnetic field along x-direction(/z-direction). p/q indicates that the same optimized structure occurred p times starting from q different initial contidions. Results have been obtained by carrying out structure optimization calculations within noncollinear approximation using PAW potentials. Mn_7 is not stable in the planar ZZ structure.

ZZ		Sc	Ti	V	Cr	Mn	Co	Ni
$n=2$	E_c	0.85	1.55	1.57	0.52	0.45	1.49	1.57
	$(\mu_x,\mu_y,$	(2.3, 2.3,	(0.0, 0.0,	(1.2, 1.2,	(0.0, 0.0,	(5.8, 4.9,	(2.8, 2.8,	(1.7, 1.0,
	$\mu_z)$, μ	2.3), 4.0	2.0), 2.0	1.2), 2.0	0.0), 0.0	6.6), 10.0	0.0), 4.0	0.0), 2.0
	$E_G/E_G^x/E_G^z$	0.49/0.18/0.17	0.36/0.36/0.36	0.67/0.67/0.66	0.56/1.87/1.87	0.18/0.18/0.18	0.05/0.05/0.05	0.18/0.17/0.3
	MO	FM	FM	FM	AFM	FM	FM	FM
	$\triangle E_{so}^x/\triangle E_{so}^z$	3.60/3.80	4.70/3.90	8.30/8.00	10.90/10.90	13.10/13.30	0.01/9.90	33.30/32.50
	$(p/q=5)$	4	4	5	3	3	5	4
$n=3$	E_c	1.36	2.00	1.90	0.71	0.68	1.89	2.01
	$(\mu_x,\mu_y,$	(0.7, 0.7,	(2.2, 2.2,	(0.6, 0.6,	(5.6, 2.2,	(1.4, -2.6,	(0.3, 0.7,	(1.2, 1.2,
	$\mu_z)$, μ	-0.3), 1.0	2.5), 4.0	0.6), 1.0	0.0), 6.0	0.0), 3.0	7.0), 7.0	1.1), 2.0
	$E_G/E_G^x/E_G^z$	0.37/0.37/0.37	0.26/0.26/0.25	0.44/0.44/0.44	1.01/1.01/1.01	0.25/0.24/0.24	0.34/0.11/0.12	0.11/0.11/0.10
	MO	FM	FM	FM	FM	FM	FM	FM
	$\triangle E_{so}^x/\triangle E_{so}^z$	3.70/3.70	4.70/4.70	8.40/8.40	10.40/10.50	13.10/13.00	8.20/9.60	33.10/32.70
	$(p/q=5)$	4	2	3	2	1	1	5
$n=4$	E_c	1.60	2.36	2.34	0.88	1.01	2.28	2.30
	$(\mu_x,\mu_y,$	(0.6, 1.7,	(1.2, 1.2,	(0.0, 0.0	(0.0, 0.0	(0.0, 0.0,	(4.6, 4.6,	(-0.8, -2.0
	$\mu_z)$, μ	0.9), 2.0	1.2), 2.0	0.0), 0.0	0.0), 0.0	0.0), 0.0	4.6), 8.0	3.4), 4.0
	$E_G/E_G^x/E_G^z$	0.29/0.29/0.29	0.41/0.41/0.41	0.28/0.28/0.28	1.09/1.09/1.09	0.30/0.30/0.30	0.03/0.03/0.03	0.06/0.21/0.20
	MO	FM	FM	AFM	AFM	AFM	FM	FM
	$\triangle E_{so}^x/\triangle E_{so}^z$	3.70/3.70	4.70/4.70	8.40/8.40	10.30/10.20	13.20/13.20	8.30/8.80	32.10/32.20
	$(p/q=5)$	3	4	2	1	3	5	2
$n=5$	E_c	1.67	2.48	2.46	0.99	1.21	2.49	2.30
	$(\mu_x,\mu_y,$	(0.8, 0.2	(0.0, 0.0	(0.7, 0.5	(2.5, 2.45,	(-1.3, 1.8,	(-2.4, 10.6,	(2.0, 3.3,
	$\mu_z)$, μ	0.6), 1.0	0.0), 0.0	0.6), 1.0	1.9), 4.0	-2.0), 3.0	-1.4), 11.0	1.1), 4.0
	$E_G/E_G^x/E_G^z$	0.26/0.26/0.26	0.34/0.34/0.34	0.27/0.27/0.27	0.28/0.44/0.44	0.09/0.21/0.21	0.33/0.33/0.33	0.21/0.20/0.20
	MO	FM	AFM	FM	FM	FM	FM	FM
	$\triangle E_{so}^x/\triangle E_{so}^z$	3.80/3.50	4.80/4.80	8.20/8.20	10.40/10.40	14.10/13.00	8.90/8.90	32.40/31.80
	$(p/q=5)$	4	4	3	1	1	2	5
$n=6$	E_c	1.74	2.53	2.57	1.24	1.30	2.55	2.45
	$(\mu_x,\mu_y,$	(0.0, 0.0,	(0.0, 0.0,	(0.0, 0.0,	(0.0, 0.0,	(0.0, 0.0,	(6.73, 6.73,	(0.0, 0.0,
	$\mu_z)$, μ	0.0), 0.0	0.0), 0.0	0.0), 0.0	0.0), 0.0	0.0), 0.0	7.31), 12.0	0.0), 0.0
	$E_G/E_G^x/E_G^z$	0.19/0.19/0.19	0.32/0.32/0.32	0.38/0.38/0.37	0.77/0.77/0.77	0.48/0.48/0.48	0.20/0.20/0.20	0.20/0.17/0.17
	MO	AFM	AFM	AFM	AFM	AFM	FM	AFM
	$\triangle E_{so}^x/\triangle E_{so}^z$	3.70/3.70	4.70/4.70	8.10/8.10	10.30/10.30	13.20/13.30	8.00/8.40	32.30/32.30
	$(p/q=5)$	1	4	5	1	4	5	5
$n=7$	E_c	1.81	2.60	2.56	1.13		2.64	2.57
	$(\mu_x,\mu_y,$	(5.2, 5.2,	(1.1, 2.8,	(0.6, 0.6,	(-0.2, 0.6,		(8.7, 8.7,	(4.7, 4.6
	$\mu_z)$, μ	5.2), 9.0	0.0), 3.0	0.6), 1.0	6.0), 6.0		8.7), 15.0	4.6), 8.0
	$E_G/E_G^x/E_G^z$	0.15/0.15/0.15	0.19/0.19/0.20	0.23/0.23/0.23	0.39/0.39/0.39		0.09/0.09/0.09	0.01/0.05/0.05
	MO	FM	FM	FM	FM		FM	FM
	$\triangle E_{so}^x/\triangle E_{so}^z$	3.80/3.80	4.90/4.80	8.20/8.20	10.60/10.40		8.30/8.50	32.50/32.20
	$(p/q=5)$	2	1	5	2		5	5

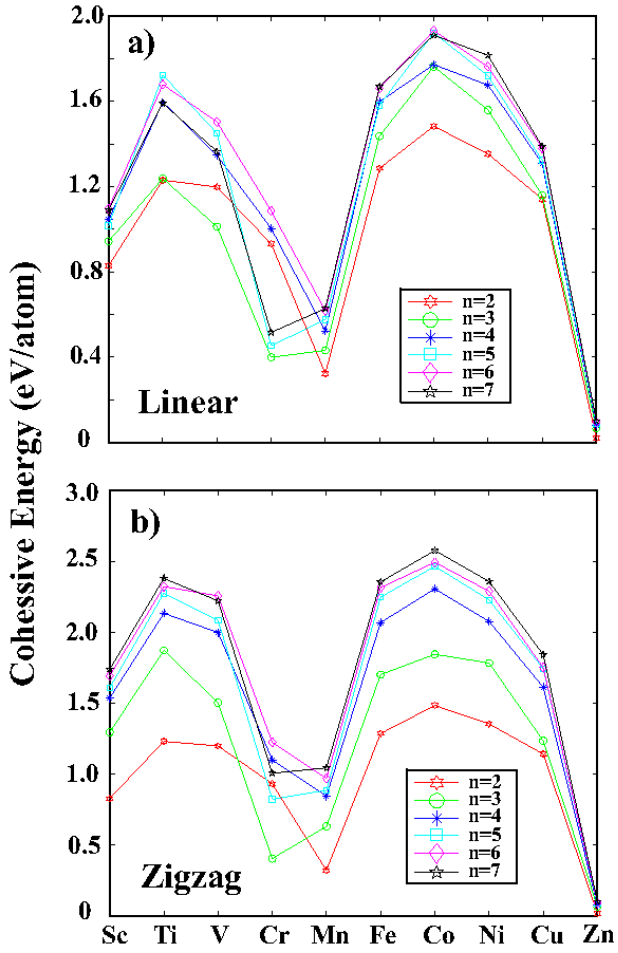

FIG. 9: (Color online) Variation of the average cohesive energy of small segments of chains consisting of n atoms. (a) The linear chains; (b) the zigzag chains . In the plot, the lowest energy configurations for each case obtained by optimization from different initial conditions.

collinear magnetism. Frustrated antiferromagnets having triangular lattice structure, disordered systems, broken symmetry on the surface will result in noncollinear magnetism. α-Mn, spin glasses, domain walls, Fe clusters are examples of this type. Coupling the magnetic moment to the crystal structure (spin-orbit coupling) poses the magnetic anisotropy which again results in the noncollinear magnetism in the structure. Finite structures that is studied in this paper, all have low symmetry and AFM-FM coupling competition which increase the probability of observing noncollinear magnetism. There are many different approaches for implementing noncollinear magnetism, such as ASW (Augmented Spherical Wave), CPA (Coherent-Potential Approximation), LSDA (Local-Spin-Density Approximation). In our study, we use fully unconstrained approach to noncollinear magnetism.[49] The Hamiltonian of the system after making simplifications and approximations will be:

$$H^{\alpha\beta}[n,\{\mathbf{R}\}] = -\frac{1}{2}\delta_{\alpha\beta} + \tilde{v}^{\alpha\beta}_{\rm eff} + \sum_{(i,j)} |\tilde{p_i}> (\hat{D}^{\alpha\beta}_{ij} + {}^1D^{\alpha\beta}_{ij} - {}^1\tilde{D}^{\alpha\beta}_{ij}) < \tilde{p_j}|$$

Here $\tilde{v}^{\alpha\beta}_{\rm eff}$ is the effective one-electron potential which depends on the electron density and the magnetization at each site; $-\frac{1}{2}\delta_{\alpha\beta}$ stands for the kinetic energy of the system. $\hat{D}^{\alpha\beta}_{ij}$, ${}^1D^{\alpha\beta}_{ij}$ and ${}^1\tilde{D}^{\alpha\beta}_{ij}$ terms in the summation sign over augmented channels represent the correction terms for long range, effective potential and wave functions. For further details see Ref.[49,50,51,52,53,54]

The finite chains discussed in the previous section within collinear approximation will now be treated using noncollinear approximation. To this end, the structure of chains have been optimized starting from the same initial geometry (starting from a segment of n atoms extracted from the optimized infinite ZZ (or ZZD) chain placed in a supercell) and following five different initial configurations of spins on individual atoms. (i) The direction of the initial magnetic moment on the atoms are consecutively altered as $xyzy$. (ii) No preset directions are assigned to the individual atoms, they are determined in the course of structure optimization using noncollinear approximation. (iii) For each triangle, the initial magnetic moment on the atoms have a non-zero component only in the xy-plane, but $(\sum_{\triangle} \mu_a)_{xy} = 0$. (Here '$\triangle$' stands for the summation over the atoms forming a triangle) (iv) Similar to (iii), but $(\sum_{\triangle} \mu_a)_z \neq 0$. (v) In a zigzag chain, the magnetic moment of atoms on the down row are directed along z-axis, while those on the up row are directed in the opposite direction. Using these five different initial conditions on the magnetic moment of individual atoms, the initial atomic structure is optimized using both ultra-soft[40] pseudopotentials and PAW[41] potentials. We first discuss the results obtained by using ultra-soft pseudopotentials. Almost all of the total magnetic moment and the cohesive energy of the optimized structures have been in good agreement with those given in Table III (obtained within collinear approximation). However, there are some slight changes for specific finite structures. For example, Sc_7 is found to have magnetic moment of 7 μ_B in collinear approximation. Even though one of the initial condition in noncollinear calculations resulted in the same magnetic moment and energy, there is even a more energetic state (0.01 eV lower) with total magnetic moment of 9 μ_B (5.2, 5.2, 5.2). The same situation also occurred with PAW potential. Ti_5 has a special magnetic moment distribution which is the same for both ultra-soft and PAW cases and will be explained below. In collinear approximation, V_5 is noted to have zero magnetic moment, nevertheless there is a state 0.03 eV lower in energy which is FM with $\mu = 1$ μ_B (0.7, 0.7, 0.2). Even though Co_7 has the same total magnetic moment in both collinear and noncollinear case, there is a signif-

icant energy difference between two cases. Noncollinear structure of Co_7 has $\sim$ 0.4 eV lower energy with magnetic moment distribution as (8.5, 8.5, 9) μ_B. Sc_4, Sc_7, Ti_3, Ti_7, V_3, V_7, Cr_7, all structures of Mn, Fe_6 and Ni_5 have truly three dimensional (3D) magnetic moment distribution.

Finally, noncollinear (NC) calculations have been performed using PAW potentials starting with five different initial assignment of magnetic moments as described above. Most of our calculations have yielded the same magnetic moment distribution with previous calculations, but there are still few cases, which are resulted differently. Mn_7 is an exception; all structure optimization starting from different initial conditions resulted in a nonplanar geometry. Note that in collinear and noncollinear calculations using ultra-soft pseudopotential Mn_7 was stable in a local minimum corresponding to the planar zigzag geometry, but it formed a cluster when spin-orbit coupling and NC effects are taken into account. Unlike other $n = 5$ zigzag structures, Ti_5 has a unique ordering of the atomic magnetic moments. Two Ti atoms of the upper row have magnetic moments which are in opposite direction. Similarly, two Ti atoms at the ends of the lower row also have atomic magnetic moments in opposite direction, but the magnitude of moments are smaller than those of the upper row. The atom at the middle of the lower row has no magnetic moment. In $n = 6$ case, only Co_6 has a non-vanishing magnetic moment. Other atoms form dimers which are coupled in the AFM order. If we assume that the shape of $n = 6$ molecule is parallelogram, there is an AFM coupling between the atoms on both diagonals. In addition to these, remaining two atoms in the middle also coupled in the AFM order. Atoms in Sc_6, Ti_6 and V_6 have magnetic moments only in the xy-plane, whereas Cr_6, Mn_6 and Ni_6 have $3D$ magnetic moment distribution. Cr_n chains exhibit an even-odd disparity; Cr_n has an AFM ordering for even n, but it has a FM ordering for odd n. There are also cases where collinear and noncollinear calculations with ultra-soft pseudopotential resulted in an excited state for magnetic moment distribution. Although PAW potential calculations found the same magnetic ordering with collinear and ultra-soft NC cases, there are even more energetic states for Sc_6, V_4, Cr_5 and Mn_5 given in Table IV. Geometric dimerization also plays an important role in determining the average cohesive energy of the system. Interestingly the cohesive energies of V_6 and V_7; Cr_6 and Cr_7; Ni_4 and Ni_5 are not changing with n. It should be denoted that Hobbs *et. al*[49] carried out noncollinear calculations with the PAW potential on Cr_{2-5} and Fe_{2-5} finite chain structures. Here, our results are in agreement with those of Hobbs *et. al*.[49]

We calculated the spin-orbit (SO) coupling energies, $\triangle E^x_{so}$ and $\triangle E^z_{so}$, under a unit magnetic field along x- and z-direction, respectively. Here, the optimized structure of every initial condition together with the calculated magnetic moment on the individual atoms are used for the calculation of SO coupling. The optimized structures of $(TM)_n$ and atomic magnetic moments, μ_a, have been determined within noncollinear approximation using PAW potentials. The results are given in Table IV in units of meV. As it can be easily seen that SO coupling does not play an important role on the energy of the planar finite structure. However, SO coupling becomes crucial when the total magnetic moments, which happen to be oriented in different directions owing to the different initial conditions, result in the same energy. In this case SO coupling energy difference changes with respect to the direction of the applied magnetic field. In Table IV, only the most energetic configurations including the SO coupling effects are given. $\triangle E^x_{so}$ and $\triangle E^z_{so}$ appear to be independent of n except Mn_5, Co_2 and Co_3. It is also observed that when SO coupling is taken into account, LUMO-HOMO gap energies decreases as in the bulk structures. Only for Ni_4, Cr_5, Mn_5 and Ni_7, LUMO-HOMO gap increased due to the fact that the final geometry of SO coupling calculations has further relaxed slightly from that of NC calculations. We close this section by noting that PAW potential is found to be more suitable for the following reasons. First, the individual atomic character in the chain structure, as well as local magnetic moment are better represented by the PAW potential. Secondly, using PAW potential one can provide an accurate prediction of spin-orbit coupling.

V. CONCLUSION

In this paper, we presented an extensive study of the structural, electronic and magnetic properties of monatomic chains of light transition metal atoms (Sc, Ti, V, Cr, Mn, Fe, Co, Ni as well as Cu and Zn) using first-principle plane wave methods. We considered infinite and periodic chains (with linear, dimerized linear, zigzag and dimerized zigzag geometry) and small chains including 2-7 atoms. Because of end effects, we found a dramatic differences between infinite chains and finite ones. Therefore we believe that the basic understanding of monatomic TM chains have to comprise both infinite and finite structures as done in the present paper.

The infinite, dimerized linear structures have a shallow minimum only for a few TM atoms; planar zigzag and dimerized zigzag structures, however, correspond to a lower binding energy providing stability in this geometry. As for short chains consisting of 4-7 TM atoms, the planar zigzag structure is only a local minimum. The finite chains tend to form clusters if they overcome energy barriers. We found close correlation between magnetic state and geometry of chain structure. In this study, we presented the variation of binding energy as a function of lattice constant for different structures and magnetic states. We also revealed the dependence of electronic and magnetic properties on the atomic structures of chains. We found that the geometric structure influence strongly the electronic and magnetic properties of the chains. For example, infinite linear Vanadium chain becomes half-metallic upon dimerization. Similarly, infinite dimerized

and metallic Sc chain becomes half-metallic with 100% spin-polarization at the Fermi level upon transformation to zigzag structure. Furthermore, while the infinite linear Mn chain has an AFM ground state, with $\mu = \sum \mu_a = 0$, but $|\sum \mu_a^{\uparrow}| = |\sum \mu_a^{\downarrow}| = 4.40\ \mu_B$, it becomes a FM metal with $\mu = \sum \mu_a = 4.36\ \mu_B$ as a result of the structural transformation from linear to dimerized zigzag structure.

Magnetic ordering of finite-chains becomes more complex and requires a treatment using noncollinear approximation. The structure optimizations carried out using ultra-soft pseudopotentials generally result in the same cohesive energy and magnetic moment in both collinear and noncollinear approximations. However, for specific finite chains the total magnetic moments calculated by using PAW potentials with the same initial magnetic moment distribution differ dramatically from ultra-soft results. Of course, our results which covers much more than 3000 different structure optimizations may not include the lowest energy state, but indicates the importance of noncollinear treatment.

VI. ACKNOWLEDGEMENT

Part of the computational resources for this study has been provided through a grant (2-024-2007) by the National Center for High Performance Computing of Turkey, Istanbul Technical University.

* Electronic address: ciraci@fen.bilkent.edu.tr

[1] K. Tsukagoshi, B. W. Alphenaar, H. Ago,Nature **401**, 572 (1999)

[2] S. Ciraci, A. Buldum, I. P. Batra, J. Phys. Condens. Matter **13**, 568 (2001)

[3] S. Ciraci, S. Dag, T. Yildirim, O. Gulseren, J. Phys. Condens. Matter **16**, 901 (2004)

[4] Y.Mokrousov, G. Bihlmayer, S. Blügel, S.Heinze, Phys. Rev. B **75**, 104413 (2007)

[5] C.M. Schneider, J. Kirschner, Handbook of Surface Science(eds K. Horn, M. Scheffler) 511-668 (Elseiver,Amsterdam, 2000)

[6] B.J. van Wees, H. van Houten, C. W. J. Beenakker, J. G. Williamson, L. P. Kouwenhoven, D. varderMarel, C. T. Foxon, Phys Rev. Lett. **60**, 848 (1988)

[7] P. Gambardella, A. Dallmeyer, K. Maiti, M.C. Malagoli, W. Eberhardt, K.Kern, C. Carbone,Nature **416**, 301 (2002)

[8] N. Agrait, A.L. Yeyati, J.M. van Ruitenbeek,Phys. Rep 377, 81(2003)

[9] A.I. Yanson, G. Rubio-Bollinger, H.E. van den Brom, N. Agrait, J.M. van Ruitenbeek,Nature **395**, 783 (1998)

[10] H. Ohnishi, Y.Kondo, K. Takayanagi,Nature **395**, 780 (1998)

[11] M.R. Sorensen, M.Brandbyge, K.W. Jacobsen,Phys Rev. B **57**, 3283 (1998)

[12] H. Hakkinen, R.N. Barnett, U.Landman, J. Phys.Chem B. **103**, 8814 (1999)

[13] D.Sánchez-Portal, E. Artacho, J. Junquera, P. Ordejón, A. Garcia, J. M. Soler, Phys Rev. Lett. **83**, 3884 (1999)

[14] J.A. Torres, E. Tosatti, A.D. Corso, F. Ercolessi, J.J. Kohanoff, F.D. Di Tolla, and J.M. Soler, Surf. Sci. 426, L441 (1999)

[15] M. Okamoto, K. Takayanagi,Phys Rev. B **60**, 7808 (1999)

[16] V. Rodrigues, T. Fuhrer, D. Ugarte,Phys. Rev. Lett. **85**, 4124 (2000)

[17] P. Sen, S. Ciraci, A. Buldum, I. P. Batra, Phys. Rev. B **64**, 195420 (2001)

[18] P. Sen, O. Gulseren, T. Yildirim, I. P. Batra, S. Ciraci, Phys. Rev. B **65**, 235433 (2002)

[19] S. Tongay, R. T. Senger, S. Dag, S. Ciraci, Phys. Rev. Lett. **93**, 136404 (2004)

[20] O. Gurlu, H. J. W. Zandvliet, B. Poelsema, S. Dag, S. Ciraci, Pjys. Rev. B **70**, 085312 (2004)

[21] J. Dorantes-Davila, G.M. Pastor, Phys Rev. Lett. **81**, 208 (1998)

[22] A. Delin, E. Tosatti, J. Phys.: Condens. Matter **16** 8061-8074 (2004)

[23] A. Bala, T. Nautiyal, K.S. Kim, Phys Rev. B **74**, 174429 (2006)

[24] Y. Mokrousov, G. Bihlmayer, S. Heinze, S. Blügel, Phys Rev. Lett. **96**, 147201 (2006)

[25] A. Delin, E. Tosatti, Phys Rev. B **68**, 144434 (2003)

[26] M. Wierzbowska, A. Delin, E. Tosatti, Phys Rev. B **72**, 035439 (2005)

[27] S. A. Wolf, D. D. Awschalom, R. A. Buhrman, J. M.Daughton, S. von Molnár, M. L. Roukes, A. Y. Chtchelkanova,and D. M. Treger, Science **294**, 1488 (2001)

[28] E. Durgun, R. T. Senger, H. Mehrez, H. Sevincli, S. Ciraci, J.Chem. Phys. **125**, 121102 (2006)

[29] R.H. Kodama, J. Magnetism and Magnetic Materials **200** (1999) 359-372

[30] H. Kachkachi, J. Magnetism and Magnetic Materials **316** (2007) 248-254

[31] V.L. Moruzzi,Phys Rev. Lett. **57**,2211 (1986)

[32] M. Luban, J. Magnetism and Magnetic Materials **272-276** (2004) e635-e641

[33] V. Heine, J.H. Samson, C.M.M. Nex, J.Phys.F. Metal Phys. **11** (1981) 2645-2662

[34] P. Gambardella, J. Phys.: Condens. Matter **15** (2003) 2533-2546

[35] M.B. Knickelbein, Phys Rev. B **70**, 014424 (2004)

[36] R.F. Wallis, Phys Rev. **105**, 540 (1957)

[37] M. C. Payne, M. P. Teter, D. C. Allen, T. A. Arias, and J. D. Joannopoulos, Rev. Mod. Phys. **64**, 1045 (1992).

[38] Numerical computations have been carried out by using VASP software: G. Kresse, J. Hafner, Phys Rev. B **47**, R558 (1993); G. Kresse, J. Furthmuller, Phys Rev. B **54**, 11169 (1996).

[39] W. Kohn and L. J. Sham, Phys. Rev. 140, A1133 (1965); P. Hohenberg and W. Kohn, Phys. Rev. B 76, 6062 (1964).

[40] D. Vanderbilt, Phys. Rev. B **41**, R7892 (1990).

[41] G. Kresse, and D. Joubert, Phys. Rev. B **59**, 1758 (1999).

[42] J. P. Perdew, J. A. Chevary, S. H. Vosko, K. A. Jackson, M. R. Pederson, D. J. Singh, and C. Fiolhais, Phys. Rev. B **46**, 6671 (1992).

[43] M. Methfessel and A. T. Paxton, Phys. Rev. B **40**, 3616 1989.
[44] H.J. Monkhorst and J.D. Pack, Phys. Rev. B **13**, 5188, (1976).
[45] A. Sommerfeld, H. Bethe, Handbuch der Physik, Springer, Berlin, 1933
[46] J. Friedel; The Physics of Metals; Ziman, J. M., Ed.; Cambridge University Press: New York, 1969. D. G. Pettifor, Solid State Physics; Ehrenreich, H., Turnbull, D., Eds.; Academic Press: New York, 1987; Vol. 40, p 43.
[47] Introduction to Solid State Physics, C. Kittel, John Willey and Sons, New York, Chichester, Brisbane, Toronto, Singapore,7^{th} Ed., 1996)
[48] J. C. Tung, G. Y. Guo, Phys. Rev. B **76**, 094413, (2007)
[49] D. Hobbs, G. Kresse, J.Hafner, Phys. Rev. B **62**, 11556 (2000)
[50] Ph. Kurz, F. Förster, L. Nordström, G. Bihlmayer, S. Blügel, Phys. Rev. B **69**, 024415, (2004)
[51] J. Anton, B. Fricke, E. Engel, Phys. Rev. A **69**, 012505, (2004)
[52] J. Kübler, K-H Höck, J. Sticht, A. R. Williams,J. Phys. F: Met. Phys. **18**, 469-483 (1988)
[53] T. Oda, A. Pasquarello, R. Car, Phys. Rev. Lett. **80**, 3622, (1998)
[54] S. Sharma, J.K. Dewhurst, C. Ambrosch-Draxl, S. Kurth, N. Helbig, S. Pittalis, S. Shallcross, L. Nordström, E. K. U. Gross, Phys. Rev. Lett. **98**, 196405, (2007)